Dalton Transactions

ROYAL SOCIETY OF CHEMISTRY

PAPER

View Article Online
View Journal

Cite this: DOI: 10.1039/d6dt00964f

Triphenylene chromophore enhances emission in Au/Cu heterometallic complexes

Jalal Ahmad,[a] Anyie P. Atencio,[a] Jas S. Ward,[b] Marianne Engeser,[c] Kari Rissanen,[b] Inmaculada Angurell[a] and Laura Rodríguez *[a]

Received 26th April 2026,
Accepted 25th May 2026

DOI: 10.1039/d6dt00964f

rsc.li/dalton

Heterometallic Au(I)–Cu(I) assemblies are attractive luminescent platforms due to synergistic metallophilic interactions and enhanced spin–orbit coupling. We report a new family of Au(I)–Cu(I) complexes incorporating a rigid 2-ethynyltriphenylene chromophore and a pyridyldiphenylphosphine auxiliary ligand. Stoichiometric reactions between a mononuclear alkynyl gold(I) precursor and Cu(I) salts bearing different counterions (PF_6^-, OTf^-, BF_4^-) afford Au_2Cu_2 assemblies whose structures and packing are strongly counterion-dependent. Single-crystal X-ray diffraction reveals Au–Cu interactions supported by Cu–N(pyridyl) and Cu···π(alkynyl) contacts. The photophysical studies show counterion-modulated dual fluorescence/phosphorescence emission in solution, with phosphorescence enhanced under inert conditions. Upon immobilization in polymer matrices, all heterometallic complexes display efficient room-temperature phosphorescence with quantum yields of up to 40% and millisecond lifetimes. These results highlight the role of counterions and matrix rigidification in controlling excited-state deactivation in heterometallic coinage-metal systems.

Introduction

Heterometallic coinage-metal clusters, particularly those combining gold(I) and copper(I), continue to attract considerable attention due to their intriguing photophysical properties arising from metallophilic interactions and ligand–metal cooperativity. The d^{10}–d^{10} contacts between Au(I) and Cu(I) centres not only stabilize unusual architectures, but also modify significantly their photophysical properties promoting efficient spin–orbit coupling (SOC), enabling room-temperature phosphorescence (RTP) and thermally activated delayed fluorescence (TADF).[1–13] The development of new materials containing both metallophilic interactions and specific chromophores allows the fine tuning of the resulting luminescence properties. Hence, Au–Cu systems appear as promising candidates for light-emitting devices, sensors, and photocatalytic singlet oxygen generation.[1,14–17]

Recent studies have demonstrated the potential of chiral and polynuclear Au–Cu(I) assemblies stabilized by phosphine or N-heterocyclic carbene ligands to deliver intense and tunable emissions. For example, chiral NHC-stabilized Au(I)–Cu(I) clusters have achieved exceptional circularly polarized luminescence and EQE values of up to 20.8% in CP-OLEDs,[15] while other Au_2Cu_2 and Au/M heterometallic systems display near-unity photoluminescence quantum yields and microsecond-scale phosphorescence lifetimes, evidencing the strong influence of metal–metal coupling on excited-state dynamics.[16,18–20] Moreover, the photophysical response has been shown to depend critically on counterions and crystal packing, which modulate intermolecular π–π interactions and metallophilic contacts.[2–4,17–19]

The incorporation of extended aromatic chromophores, such as polycyclic acenes or triphenylene derivatives, provides an effective strategy to enhance the intraligand (IL) absorption and emission characteristics while promoting π-stacking in the solid state.[21] Triphenylene, with its rigid planar structure and high photostability, can act as both a light-harvesting antenna and a scaffold for supramolecular organization, favouring aggregation-induced emission (AIE) and energy migration phenomena.[22,23] Despite these advantages, Au–Cu clusters supported by triphenylene-based alkynyl ligands remain unexplored, particularly regarding the interplay between ligand rigidity, counterion identity, and luminescence behaviour.

In this work, we report the synthesis, structural characterization, and photophysical properties of a new family of Au(I)–Cu(I) heterometallic complexes incorporating a 2-ethynyltriphenylene chromophore and the pyridyldiphenylphosphine (PPh_2Py) auxiliary ligand. These systems form Au_2Cu_2 cores linked through Cu–N(pyridyl) and Cu···π(C≡C) interactions, with the overall structure and packing modulated by the counterion (PF_6^-, OTf^-, or BF_4^-). The different size and shape of

[a]Departament de Química Inorgànica i Orgànica, Secció de Química Inorgànica, Universitat de Barcelona and Institut de Nanociència i Nanotecnologia (IN2UB), Martí i Franquès 1-11, E-08028 Barcelona, Spain. E-mail: laurarodriguezr@ub.edu
[b]University of Jyvaskyla, Department of Chemistry, 40014 Jyväskylä, Finland
[c]Kekulé-Institut für Organische Chemie und Biochemie der Universität, Gerhard-Domagk-Strassse 1, D-53121 Bonn, Germany

these counterions have been previously observed to affect the resulting structure and luminescence properties;[16] therefore, further investigation in this field is warranted. The combination of a rigid π-conjugated chromophore and metallophilic Au–Cu contacts provides a versatile platform to probe structure–property relationships in luminescent heterometallic clusters. Comprehensive photophysical studies, both in solution and in polymer matrices, reveal counterion-dependent dual emission and efficient phosphorescence under deoxygenated conditions, contributing to the understanding of excited-state dynamics in coinage-metal assemblies.

Results and discussion

Synthesis and characterization

Three different Au(I)–Cu(I) heterometallic structures were synthesized by the reaction of the previously synthesized **[Au(L)(PPyPh$_2$)]** gold(I) complex and different Cu(I)X salts (X = PF_6^- (a), OTf^- (b) and BF_4^- (c)) (Scheme 1). The gold complex contains 2-ethynyltriphenylene as the chromophore (**L**) and pyridyldiphenylphosphane as the ancillary ligand, having the pyridyl unit to coordinate to the second metal center (Schemes S1 and S2). The formation of the gold(I) complex was evidenced by the disappearance of the terminal alkynyl proton in the corresponding ^{1}H NMR spectrum and a 10 ppm downfield shift in the $^{31}P\{^1H\}$ NMR spectra (see the SI). The synthesis of the final Au(I)/Cu(I) heterometallic structures was carried out by the stoichiometric reaction of **[Au(L)(PPyPh$_2$)]** with the corresponding $[Cu(MeCN)_4]X$ salt in dichloromethane overnight at room temperature (Scheme 1B), obtaining orange-red solids with moderate yields. ^{1}H, ^{19}F, and $^{31}P\{^1H\}$ NMR and IR spectroscopies together with electrospray ionization mass spectrometry (ESI-MS) in positive and negative modes demonstrate in all cases the formation of the compounds depicted in Scheme 1 (Fig. S1–S29).

The ^{1}H NMR spectra show that the protons at the *ortho* position (H_a) to the nitrogen atom in the pyridyl ring of the phosphine are affected by the coordination of the Cu(I) center in all the cases with a 0.5–0.9 ppm downfield shift with respect to **[Au(L)(PPyPh$_2$)]** (see the SI). The broadening and downfield shift observed for the heterometallic systems is attributed to the repolarization of the heterometallic product of SOC influenced, as previously observed in other systems previously studied in the research group.[16] A solvent molecule (acetonitrile) is occupying the fourth coordination position of the pseudo-tetrahedral Cu(I) center (see Fig. S7), due to the weak coordination ability of counteranions. This solvent molecule can be replaced by water or $PF_2O_2^-$ formed by partial hydrolyzation of PF_6^- during the crystallization process (see the X-ray crystal structure of **Cu1a** and **Cu1b**). The $^{31}P\{^1H\}$ NMR spectrum exhibits a downfield shift of approximately 0.3 ppm in **Cu1b** and 7 ppm in **Cu1a** and **Cu1c**, with respect to the gold(I) precursor due to the proximity of the phosphorus atom to the Cu(I) coordination site (Fig. S14 and S16). The presence of the PF_6^- counterion in **Cu1a** is evidenced by the

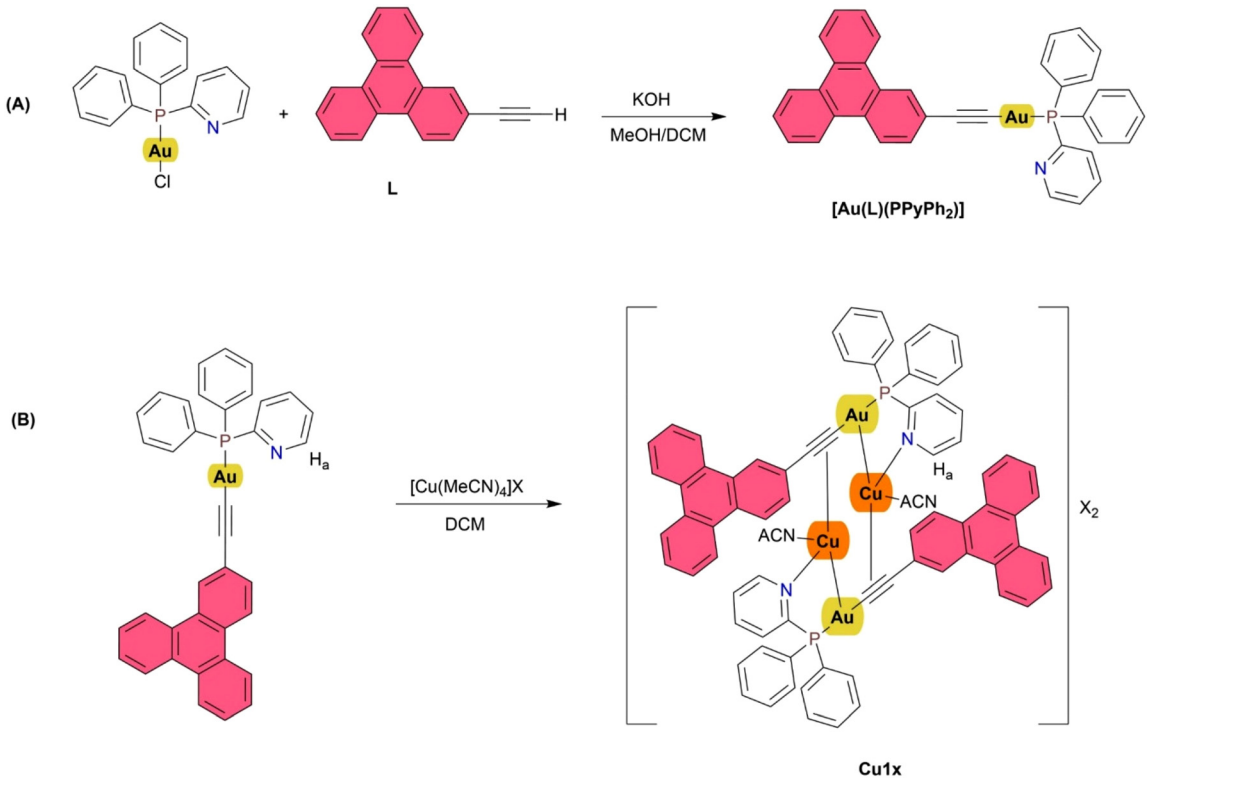

Scheme 1 Synthesis of the gold(I) precursors (A) and their Cu(I)/Au(I) derivatives (B). X = PF_6^- (a), OTf^- (b), BF_4^- (c). ACN: acetonitrile molecules.

septuplet at −144.3 ppm ($^1J_{PF}$ = 707 Hz). The IR spectra of the heterometallic systems display very weak and broad ν(C≡C) vibrations, a sign of Cu···π(C≡C) coordination being present.

High resolution mass spectra show evidence for the formation of the tetranuclear compounds ($Au_2Cu_2L_2$) in all cases with a signal for a cation [M-anion]$^+$ and a series of fragments thereof. ESI spectra recorded under soft conditions additionally show some unspecific aggregation to polynuclear gold complexes, and the spectra are dominated by a strong signal for the cationic diphosphane complex Au$(PPyPh_2)_2^+$, both observations are very typical of ESI mass spectra of solutions containing gold(I) and phosphanes (Fig. 1 and S25–S29).

Single-crystal X-ray diffraction provided the final and unambiguous structural information for **[Au(L)(PPyPh$_2$)]** and the heterometallic systems **Cu1a** and **Cu1b**. The corresponding structures are presented in Fig. 2, 3 and S30–S33 and the selected bond lengths and angles are summarized in Table S1. The packing of the **[Au(L)(PPyPh$_2$)]** complex is governed by C–H···π interactions between the triphenylene aromatic unit and a phenyl ring of a neighboring molecule. No aurophilic interactions are observed (minimum Au···Au distances of 5.21 Å, Table S1). The structure of **Cu1a** and **Cu1b** shows a heterometallic Au/Cu core where two Au–Cu direct metallophilic interactions (with Au···Cu distances in the range of 2.77–2.89 Å, Table S1) are interconnected through a $PF_2O_2^-$ molecule in **Cu1a** and a H_2O molecule in **Cu1b**, incorporated during the crystallization process by displacement of the position occupied by acetonitrile (see above, NMR). Hydrolyzation of the PF_6^- ion is a common feature in coordination chemistry and is very difficult to avoid even working under rigorous inert atmosphere conditions. Certain metal salts, including Cu(I), are capable of catalyzing this hydrolysis in the presence of traces of water.[24,25] The copper atoms are coordinated simultaneously to the Au(I) center and nitrogen atom of the pyridyl unit of one molecule and an acetylide (Cu···π(C≡C) interactions) of a neighboring gold(I) unit (Fig. 2). The bond distances between Cu and the centroid of the triply bonded carbon atoms (Cu–C≡C$_{centroid}$) were 1.906/1.917/1.918/1.931 Å (**Cu1a**) and 1.943/1.947 Å (**Cu1b**). The difference in the bridging ligand (OH_2 in **Cu1a** *vs.* $PF_2O_2^-$ in **Cu1b**) does not affect the presence of metal···metal contacts, but provokes slight differences in the general packing.

Linear coordination of the ligands at the Au(I) centers is preserved, with P–Au–C angles of 170.08(13)/173.43(13)/173.92(15)/174.83(16)° and 174.89(12)/175.23(11)° for **Cu1a** and **Cu1b**, respectively. The angles of the C–Au–Cu bridge of 103.85(16)/106.39(15)/108.32(13)/108.72(13)° in **Cu1a** are noticeably wider than those of 92.42(11)/92.76(11)° in **Cu1b**. These angle differences are responsible for the differences observed in the packing with a less constrained structure in the case of **Cu1b**, while π···π stacking between the triphenylene groups together with C–H···π interactions between a π ring of the chromophore and the phosphine moieties is observed for **Cu1a**, giving rise to a closer packing arrangement (Fig. 3 and S31, S32). The observed packing arrangement is analogous to

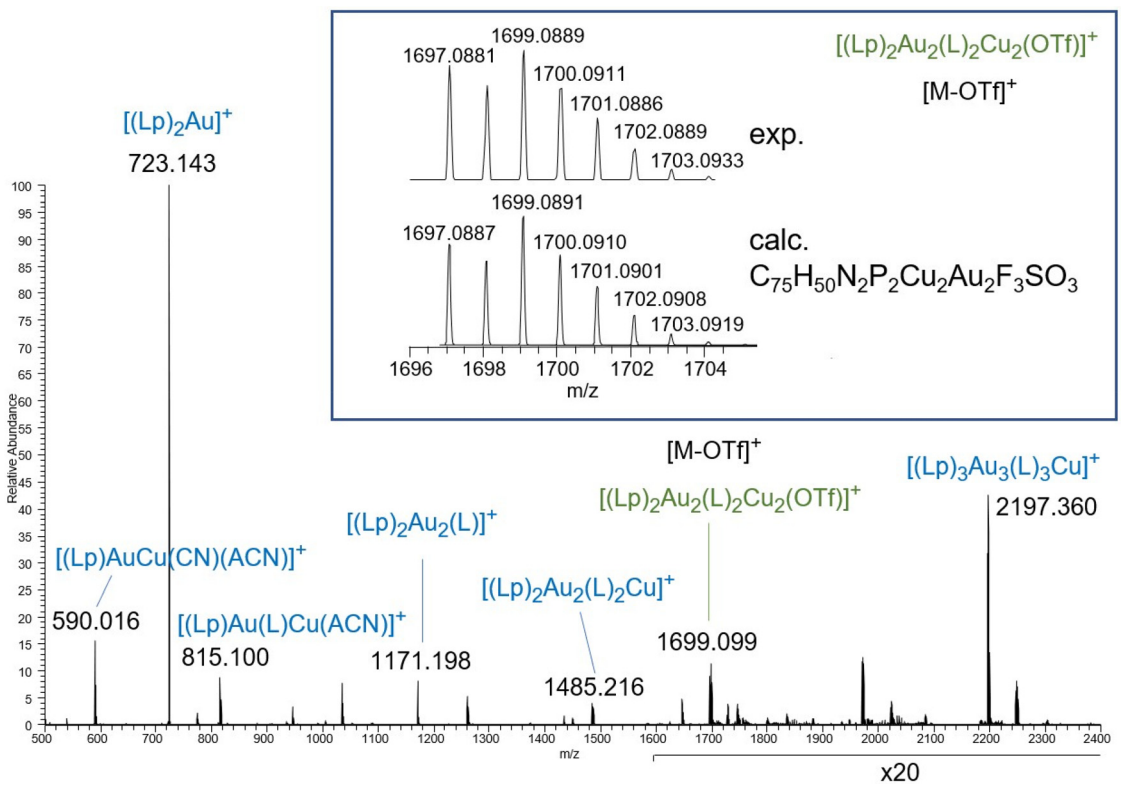

Fig. 1 HR-ESI(+) mass spectra of **Cu1b**, Lp = $PPyPh_2$.

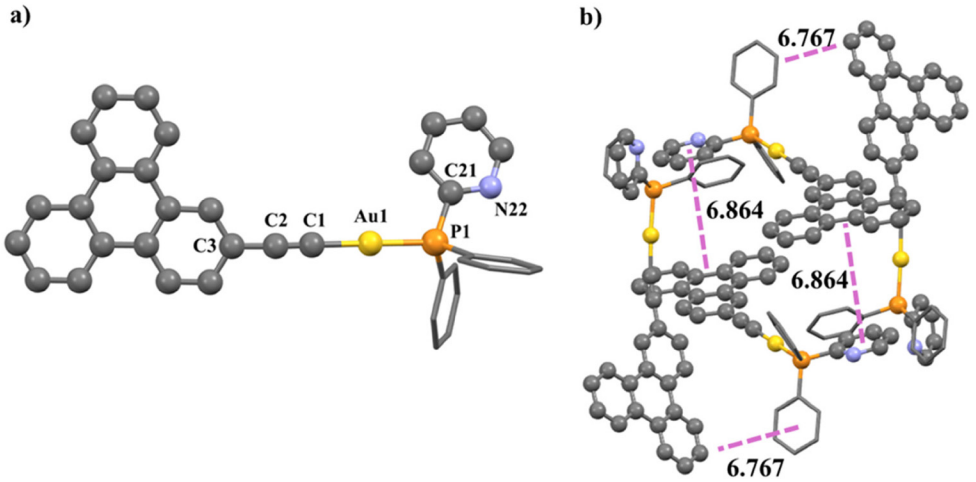

Fig. 2 (a) X-ray crystal structures of **[Au(L)(PPyPh$_2$)]**; (b) unit cell of the complex. Yellow: gold; orange: phosphorus; blue: nitrogen. Hydrogen atoms have been omitted for clarity. Purple dashed lines indicate π–π interactions. Distances are indicated in Å and have been calculated between ring centroids.

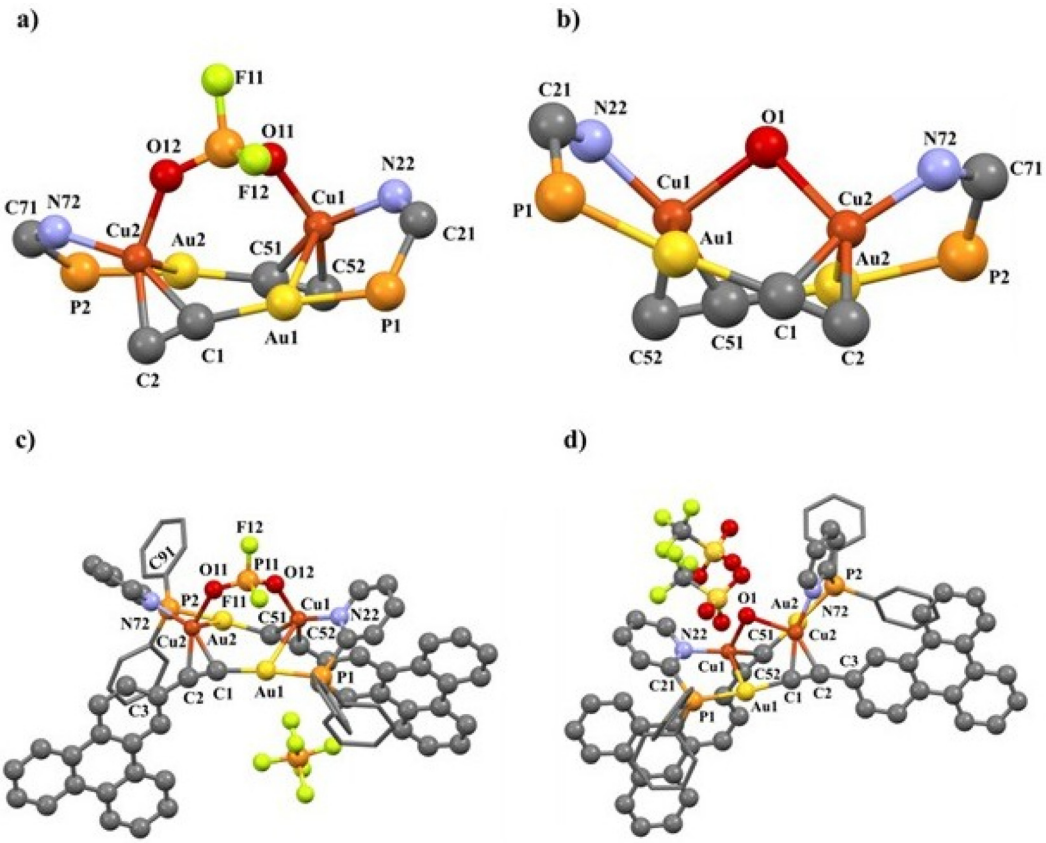

Fig. 3 Heterometallic core of **Cu1a** (a) and **Cu1b** (b). Structure of **Cu1a** (c) and **Cu1b** (d). Yellow: gold; bronze: copper; orange: phosphorus; blue: nitrogen; light green: fluorine. Hydrogen atoms have been omitted for clarity.

that previously obtained with similar compounds containing phenanthrene instead of triphenylene, compatible with the presence of a large chromophore that prevents a larger number of metallophilic contacts and the formation of a larger cluster structure.[16]

In the **Cu1a** structure, two of the four crystallographically independent triphenylene chromophore units exhibit intermolecular π–π interactions with distances of 3.34 and 3.39 Å between the calculated planes of the triphenylene substituents and centroid-to-centroid distances of 4.84 and 5.31 Å, respect-

ively. In the case of **Cu1b**, the same intermolecular π–π interaction was present for both the crystallographically independent triphenylene chromophore units with a centroid-to-centroid distance of 3.74 Å (Fig. S33).

Unfortunately, we could not grow single crystals suitable for X-ray diffraction for **Cu1c** but the HR-MS spectrum (Fig. S28 and S29) displays the same pattern for the other two complexes, supporting the formation of an analogous heterometallic complex with the counterion BF_4^-. Therefore, this does not necessarily constitute a limitation for conducting the corresponding luminescence studies in all cases.

Photophysical properties

The absorption spectra of **[Au(L)(PPyPh$_2$)]** and the corresponding Au(I)–Cu(I) heterometallic systems were recorded in 1 × 10^{-5} M CH_2Cl_2 solutions at room temperature, as shown in Table 1 and Fig. S34.

The absorption of **[Au(L)(PPyPh$_2$)]** exhibits vibronically structured bands corresponding to the alkynyltriphenylene chromophore[20,26] with peaks at around 268 nm and 318 nm attributed to π–π* intraligand transitions. The vibronic resolution is lost in the Au(I)–Cu(I) heterometallic structures due to the coordination of the second metal center (Cu(I)) to the alkynyl moiety. The observed broadening can be attributed to the existence of metallophilic contacts and the consequent cluster-centred (^{3}CC) transitions or ligand-to-metal charge transfer (LMCT) contributions.[16,27] This band is significantly less intense for **Cu1c**, likely due to its lower solubility in this solvent, which led us to investigate its photophysical properties only in the solid state.

Emission spectra were recorded for all the complexes in solution at room temperature and they display dual emission (Fig. 4). Fluorescence emission at *ca.* 380 nm is recorded for **[Au(L)(PPyPh$_2$)]** and is *ca.* 30 nm red-shifted for the heterometallic complexes. A second emission at longer wavelengths is recorded in all cases, with higher intensity for the heterometallic compounds that, as expected, becomes more important upon deoxygenation of the solutions (Fig. 4b). These bands are assigned to metal-perturbed IL emissions for **[Au(L)(PPyPh$_2$)]** (^{1}IL and ^{3}IL respectively) located at the ethynyltriphenylene unit, in agreement with the recorded Stokes' shift and emission lifetimes on the order of a few ns (fluorescence band) and microseconds (phosphorescence band), Table S4.[20,28–30]

The broadening of the lower energy emission band in the heterometallic complexes together with the recorded red-shift with respect to the Au(I) precursor let us expect a different origin, as previously observed with other Au/Cu heterometallic structures containing the same $PPyPh_2$ phosphane. These transitions have been attributed to a combination of IL/LL′/LAuMCT excited states origin.[17] In particular, the ligand-to-metal charge-transfer nature of these transitions has previously been assigned on the basis of time-dependent density functional theory (TDDFT) calculations. Moreover, this charge-transfer contribution was found to be enhanced in the heterometallic compounds compared to the homometallic analogues, highlighting the key role of the copper centre, being in agreement with the recorded red-shift.[17,31,32]

The major contribution of phosphorescence recorded for **Cu1a** with respect to **Cu1b** may be ascribed to the more compact packing (according to X-ray crystal data) and the slightly shorter distance between the Cu and the alkynyl moiety of the chromophore, favoring the heavy atom effect and intersystem crossing.

Table 1 Absorption and emission data of the complexes in dichloromethane in 1 × 10^{-5} M under air-equilibrated conditions and N_2-saturated conditions

Complex	Absorption λ_{max}, nm (ε × 10^4 M^{-1} cm^{-1})	Fluorescence emission, λ_{max} (nm)	Phosphorescence emission, λ_{max} (nm)	I_{Phos}/I_{Fl} (air)	I_{Phos}/I_{Fl}, Sat-N_2
[Au(L)(PPyPh$_2$)]	257 (6.83), 268 (0.78), 277 (7.83), 310 (3.96), 327 (5.19)	379	481	0.1	2.2
Cu1a	259 (6.00), 268 (5.99), 326 (2.39), 346 (2.44)	416	545	0.8	5.7
Cu1b	258 (8.15), 268 (8.09), 327 (2.97), 347 (3.01)	411	537	0.3	2.0

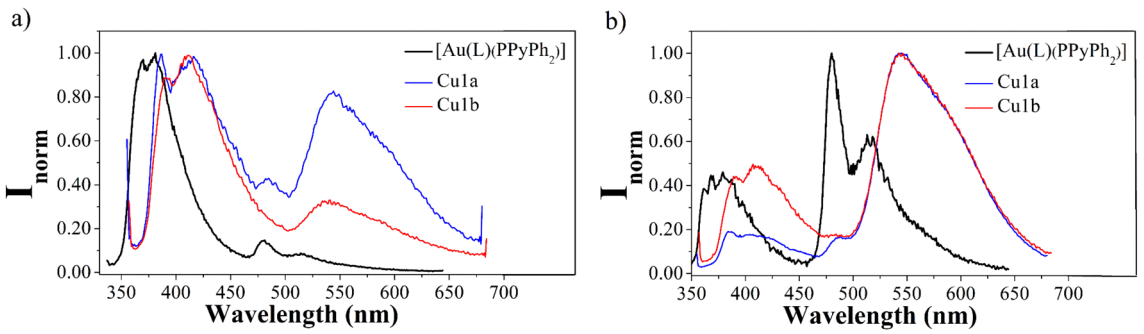

Fig. 4 Normalized emission spectra of the complexes under (a) air-equilibrated conditions; (b) N_2-saturated conditions in 1 × 10^{-5} M dichloromethane solutions, λ_{exc} = 345 nm.

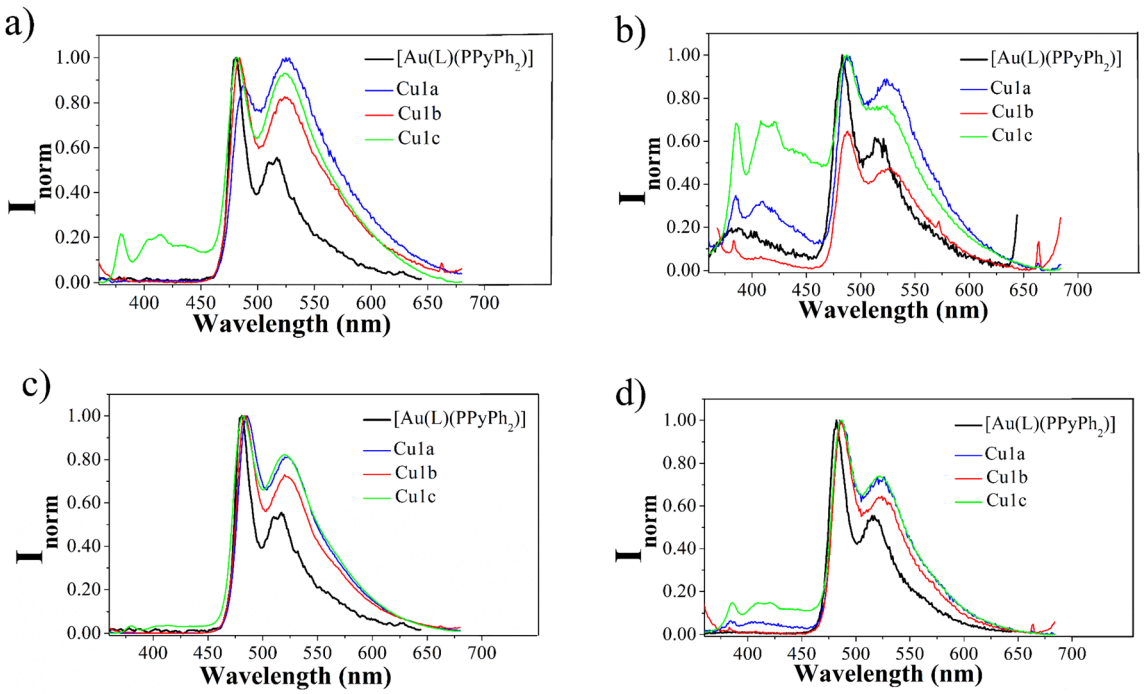

Fig. 5 Normalized emission spectra of complexes under air-equilibrated conditions in (a) PMMA matrix; (b) PS matrix; and under N_2-saturated conditions in (c) PMMA matrix; (d) PS matrix.

The compounds are weaky emissive in the solid state with a main contribution of fluorescence for **[Au(L)(PPyPh$_2$)]** and almost pure room temperature phosphorescence for the three Au/Cu complexes with a broad shape due to the formation of aggregates (Fig. S35 and Table S6).

The emission properties of the compounds were improved when they are immobilized in organic matrixes, due to the restriction of the non-radiative deactivation pathways.[33–36] Additionally, this method allows the samples to be more dispersed, preventing the strong aggregation observed in the solid state and leading to better-resolved spectra with enhanced emission efficiency. Polystyrene, PS, and poly(methyl methacrylate), PMMA, were then doped with 1% of the compounds. It was observed in all cases either pure room temperature phosphorescence, that is the emission band at longer wavelengths, *ca.* 550 nm (in PMMA) or the major component of this emission (PS) being fluorescence almost negligible in all cases upon deoxygenation of the samples, due to the phosphorescence enhancement (Fig. 5 and Table S7). The emission efficiency has been clearly improved up to 30–40% in PMMA (Table S8), which is larger than others previously investigated in our group for gold(I) and Au–Cu structures.[17] Very long emission lifetimes have been recorded of hundreds of μs (Table S9), which are longer in the order of previously reported heterometallic Au/M (M = Cu, Ag) clusters.[17,37–42]

Conclusions

The formation of discrete Au_2Cu_2 assemblies is promoted by the cooperative coordination of the pyridyl and alkynyl fragments to Cu(I), together with Au–Cu metallophilic interactions. The resulting stoichiometry of the complexes is induced by the large size of the ethynyltriphenylene chromophore. Single-crystal X-ray diffraction revealed that the counterion plays a decisive role in determining the overall molecular arrangement and intermolecular packing, modulating π–π interactions between triphenylene units and the accessibility of the metallic core.

Photophysical investigations highlighted the impact of heterometallic coupling on the excited-state behavior. While weak emission is recorded in dichoromethane solution, this property is clearly enhanced by restriction of non-radiative deactivation channels upon immobilization of the samples in PMMA and PS matrixes. This immobilization allows an enhancement of the phosphorescence emission quantum yield in a factor of 10× (from 4 to 40%) and very long emission decay times of up to hundreds of μs.

Interestingly, the use of the triphenylene chromophore has induced a clear advantage in the development of efficient room temperature phosphorescence emitters with denoted photophysical properties with respect to previous data reported in the literature.

Experimental section

General procedures

All manipulations have been performed under pre-purified N_2 using standard Schlenk techniques. Solvents have been distilled from appropriate drying agents. Commercial reagents

2-bromotriphenylene, 2-(diphenylphosphino)pyridine ($PPyPh_2$), KOH, and copper salts $[Cu(MeCN)_4]PF_6$, $[Cu(MeCN)_4]OTf$, $[Cu(MeCN)_4]BF_4$ were purchased from Aldrich and used as received.

Physical measurements

Infrared spectra were recorded using an FT-IR 520 Nicolet Spectrophotometer. ^1H NMR (δ (TMS) = 0.0 ppm), $^{31}P\{^1H\}$ NMR (δ (85% H_3PO_4) = 0.0 ppm) and ^{19}F NMR spectra were recorded at 400 or 500 MHz using Varian and Bruker spectrometers at 25 °C (Centres Científics i Tecnològics, Universitat de Barcelona). *J* values are given in Hz. HR-ESI mass spectra have been recorded with a Thermo Fisher Scientific Orbitrap XL and a Bruker micrOTOF-Q mass spectrometer from acetonitrile solution. Absorption spectra were obtained in a 10 mm quartz cuvette in dichloromethane on a Varian Cary 100 Bio UV Spectrophotometer. The emission spectra of the compounds in solution were obtained in a fluorescence quartz cuvette of 10 mm path length, using a Horiba-JobinYbon SPEX Nanolog Spectrofluorimeter (Universitat de Barcelona). Quantum yields have been recorded on an Absolute PL quantum yield spectrometer from Hamamatsu Photonics upon excitation of the samples at 310–345 nm. Luminescence lifetimes were measured on a JYF-DELTAPRO-NL equipment upon excitation of the samples with a 284 nm NanoLED and collecting the decays through a bandpass filter of 400, 500, or 550 nm, depending on the emission maximum. The best fittings correspond to biexponential decays, and the indicated values correspond to the average considering the respective amplitudes.

The single crystal X-ray data for all crystals were collected at 120 K using a Rigaku Synergy or Agilent SuperNova diffractometer both fitted with a HyPix-Arc 100 detector using mirror-monochromated Cu-Kα (λ = 1.54184 Å) radiation. The structures were solved by intrinsic phasing (SHELXT)[43] and refined by full-matrix least squares on F^2 using Olex2,[44] utilizing the SHELXL module.[45] Anisotropic displacement parameters were assigned to non-H atoms and isotropic displacement parameters for all H atoms were constrained to multiples of the equivalent displacement parameters of their parent atoms with $U_{iso}(H) = 1.2U_{eq}(C)$ of their respective parent atoms. The experimental details for the data collections of **[Au(L)(PPyPh$_2$)]**, **Cu1a**, and **Cu1b** are given in Table S1. Deposition numbers 2481587, 2520370 and 2520371 contain the supplementary crystallographic data for this paper.

Synthesis and characterization

Synthesis of 2-ethynyltriphenylene (L). The following synthesis has two parts: *first part*: 2-bromotryphenylene (0.500 g, 0.770 mmol), dichloridebis(triphenylphosphine)palladium(II) (0.054 g, 0.077 mmol) and triphenylphosphine (0.010 g, 0.038 mmol) were added in a Schlenk tube. Under nitrogen, a mixture (4 : 1) of tetrahydrofuran (24 ml) and triethylamine (6 ml) was added. The resulting solution was stirred for 2 h at 40 °C. Next, copper(I) iodide (0.015 g, 0.077 mmol) was added to the Schlenk tube, and the resulting solution was stirred for 15 minutes at 40 °C. Finally, ethynyltrimethylsilane (0.66 ml, 4.6 mmol) was added, and the resulting solution was stirred overnight at 60 °C, and then at 85 °C for 4 h. The reaction mixture was allowed to reach room temperature, and the volatiles were removed under vacuum. The solid obtained was purified through a chromatographic column as follows: a first column where the stationary phase was silica and the eluent was a mixture (1 : 1) of hexane and dichloromethane. This column was used as a precolumn to separate the palladium residues. A second column where the stationary phase was silica, and the eluent was a mixture (9 : 1) of hexane and dichloromethane. This second column allowed the separation of the desired product: trimethyl(triphenylen-2-ylethynyl)silane. *Second part*: trimethyl(triphenylen-2-ylethynyl)silane (0.095 g, 0.290 mmol) was dissolved in a mixture (1 : 2) of methanol (10 ml) and tetrahydrofuran (20 ml) in a Schlenk tube. Potassium fluoride dihydrate (0.191 g, 2.03 mmol) was added to the Schlenk tube, and the resulting solution was stirred for 2 h at room temperature. The volatiles were removed under vacuum. Then, the organic phase was extracted with dichloromethane, washed with water, and dried with anhydrous magnesium sulfate. The reaction mixture was filtered. The whitish solid obtained was dried under vacuum: 2-ethynyltriphenylene. Yield: 93%. IR ($\bar{\nu}$, cm^{-1}): 3265 (ν C≡CH), 2959 (ν CH), 2160 (ν C≡C), 1488 (δ CH). δ_H (400 MHz, $CDCl_3$) 8.82 (d, *J* = 1.6, 1H, H_1), 8.68–8.58 (m, 5H, H_3–H_{11}), 7.75 (dd, *J* = 8.5, *J* = 1.6, 1H, H_2), 7.72–7.64 (m, 4H, H_3–H_{11}), 3.23 (s, 1H, (CCH (ethynyl))).

Synthesis of the Au(I) complexes

Synthesis of [AuCl(PPyPh$_2$)]. Diphenyl-2-pyridyl phosphane ($PPyPh_2$) (0.212 g, 0.81 mmol) and [AuCl(tht)] (0.259 g, 0.81 mmol) were dissolved in 5 mL of dichloromethane and stirred for 1 h at RT; the resultant mixture was precipitated by adding 10 ml of hexane and filtered *via* a cannula to get the desired product. Yield: 92%. IR ($\bar{\nu}$ cm^{-1}): 3058 (ν CH), 1568 (ν C═N), 1477 (ν C═C), 1311 (ν CN), 1176 + 1157 (δ P–Ph). δ_H (400 MHz, $CDCl_3$) 8.79 (d, *J* = 4.7, 0.9, 1H, H_a), 7.99 (t, *J* = 7.8, 1.1, 1H, H_d), 7.83–7.77 (m, 1H, H_c), 7.74–7.65 (m, 4H, Ph), 7.56–7.43 (m, 6H, Ph), 7.42–7.37 (m, 1H, H_b). δ_P (162 MHz, $CDCl_3$) 32.3.

Synthesis of [Au(L)(PPyPh$_2$)]. 2-Ethynyl triphenylene (**L**) (0.051 g, 0.20 mmol) was added to a methanol (10 mL) solution of KOH (0.023 g, 0.40 mmol). The mixture was stirred for 2 h at RT. Then, a solution of **[AuCl(PPyPh$_2$)]** (0.100 g, 0.20 mmol) in 10 mL of dichloromethane was slowly added. The solution was left overnight with rigorous stirring at RT after which the solvents were removed under vacuum. The mixture was vacuum dried and then dissolved in a minimal amount of dichloromethane to pass it through celite; the filtrate from the celite column was dried to a minimal amount and 5 mL of diethyl ether was added to precipitate the white solid of the complex. Yield: 58%. IR ($\bar{\nu}$ cm^{-1}): 3051 (ν CH), 2112 (ν C≡C), 1604 (ν C═C), 1569 (ν C═N), 1480–1446 (δ CH), 1182 (ν CN), 1099 (δ CN), 1045 + 1030 (δ CH). δ_H (400 MHz, $CDCl_3$) 8.85 (d, *J* = 1.6, 1H, H_1), 8.81 (d, *J* = 4.7, 1H, H_a),

8.67–8.58 (m, 4H, H_4–H_{11}), 8.55 (d, J = 7.8, 1H, H_3), 8.08 (t, J = 1.1, 1H, H_d), 7.84–7.73 (m, 6H, H_c, H_2, Ph), 7.68–7.60 (m, 4H, H_4–H_{11}), 7.56–7.44 (m, 6H, Ph), 7.42–7.36 (m, 1H, H_b). δ_P (162 MHz, $CDCl_3$) 41.3. ESI-MS (+) m/z: (Lp = $PPyPh_2$, L = chromophore ligand $C_{20}H_{11}$): 1171.191 $[2M–Lc]^+$, 501.079 $[(Lp)Au(ACN)]^+$, 723.139 $[(Lp)_2Au]^+$, 1434.278 $[(Lp)_3Au_2(L)]^+$, 1883.332 $[(Lp)_3Au_3(L)_2]^+$.

Synthesis of the Au(I)–Cu(I) complexes

$[Au_2Cu_2(L)_2(PPyPh_2)_2][PF_6]_2$ (Cu1a). [Au(L)($PPyPh_2$)] (0.020 g, 0.028 mmol) was added in 3 mL of dichloromethane and stirred for 5 min. Then $[Cu(MeCN)_4]PF_6$ (0.011 g, 0.028 mmol) previously dissolved in 2 mL of dichloromethane was added. The addition of $[Cu(MeCN)_4]PF_6$ causes a sudden change of colour to bright orange. After overnight rigorous stirring, the solution was dried under vacuum and the residue was dissolved in 2 mL of dichloromethane and precipitated with 4 mL of hexane. Complex **Cu1a** was obtained as a light orange solid. Yield: 85%. IR ($\bar{\nu}$ cm^{-1}): 3082 + 2965 (ν CH), 2217 (ν C≡C), 1670 (ν C=N), 1607 (ν C=C), 1485 + 1438 (δ CH), 1285 + 1261 (ν CN), 833 (ν PF). δ_H (400 MHz, CD_3COCD_3) 9.55 (d, J = 5.3, 2H), 8.97–8.64 (m, 2H), 8.50–8.28 (m, 4H), 8.18–7.97 (m, 4H), 7.94–7.63 (m, 41H), 7.59–7.31 (m, 6H). δ_P (162 MHz, CD_3COCD_3) 47.4, −144.3 (hept, J = 707). δ_F (376 MHz, $CDCl_3$) −67.3 (d, J = 707). ESI-MS (+) m/z: (Lp = $PPyPh_2$, L = chromophore ligand $C_{20}H_{11}$): 1695.102 $[M–PF_6]^+$, 590.013 $[(Lp)AuCu(ACN)(CN)]^+$, 723.140 $[(Lp)_2Au]^+$, 1035.043 $[(Lp)_2Au_2Cu(CN)_2]^+$, 1485.211 $[(Lp)_2Au_2(L)_2Cu]$, 2197.353 $[(Lp)_3Au_3(L)_3Cu]^+$. HR ESI-MS: 1693.1019 $[M–PF_6]^+$, calculated for $C_{74}H_{50}N_2P_3Cu_2Au_2F_6$: 1693.1009.

$[Au_2Cu_2(L)_2(PPyPh_2)][OTf]_2$ (Cu1b). [Au(L)($PPyPh_2$)] (0.020 g, 0.028 mmol) was added in 3 mL of dichloromethane and stirred for 5 min. Then $[Cu(MeCN)_4]OTf$ (0.012 g, 0.028 mmol) previously dissolved in 2 mL of dichloromethane was added. The addition of $[Cu(MeCN)_4]OTf$ causes a sudden change of color to bright orange. After 4 h of rigorous stirring, the solution was dried under vacuum. The solid was dissolved in 2 mL of dichloromethane and precipitated with 4 mL of hexane. Complex **Cu1b** was obtained as a brown solid. Yield: 80%. IR ($\bar{\nu}$ cm^{-1}): 3072 (ν CH), 1938 (ν C≡C), 1610 (ν C=N), 1586 (ν C=C), 1482–1436 (δ CH), 1223 (ν CF), 1158 (ν CN), 1023 (ν S=O). δ_H (400 MHz, $CDCl_3$) 9.76 (s, 2H), 8.74–8.57 (m, 4H), 8.52 (d, J = 7.9, 2H), 8.24 (d, J = 8.6, 2H), 8.15 (s, 4H), 7.92 (s, 2H), 7.84–7.58 (m, 10H), 7.76–7.61 (m, 15H), 7.20–6.82 (m, 8H). δ_P (162 MHz, $CDCl_3$) 41.9. δ_F (376 MHz, $CDCl_3$) −77.9. ESI-MS (+) m/z: (Lp = $PPyPh_2$, L = chromophore ligand $C_{20}H_{11}$): 1699.099 $[M–OTf]^+$, 590.016 $[(Lp)_2AuCu(ACN)(CN)]^+$, 723.143 $[(Lp)_2Au]^+$, 815.100 $[(Lp)Au(L)Cu(ACN)]^+$, 1171.199 $[(Lp)_2Au_2(L)]^+$, 1485.216 $[(Lp)_2Au_2(L)_2Cu]^+$, 2197.353 $[(Lp)_3Au_3(L)_3Cu]^+$. HR ESI-MS: 1697.0881 $[M–OTf]^+$, calculated for $C_{75}H_{50}N_2P_2Cu_2Au_2F_3SO_3$: 1697.0887.

$[Au_2Cu_2(L)_2(PPyPh_2)_2][BF_4]_2$ (Cu1c). A similar procedure used for complex **Cu1a** was followed for the synthesis of complex **Cu1c**, but using $[Cu(MeCN)_4]BF_4$ instead of using $[Cu(MeCN)_4]PF_6$. The complex was obtained as a red solid. Yield: 95%. IR ($\bar{\nu}$ cm^{-1}): 3075 (ν CH), 1974 (ν C≡C), 1609 + 1587 (ν C=N), 1482 (ν C=C), 1287 (δ CH), 1052 + 633 + 617 (ν BF). δ_H (400 MHz, CD_3COCD_3) 9.36 (s, 1H), 8.66 (d, J = 8.0, 3H), 8.56 (d, J = 7.9, 2H), 8.45–8.36 (m, 2H), 8.19 (d, J = 8.6, 4H), 7.93–7.77 (m, 4H), 7.74–7.24 (m, 41H). δ_P (162 MHz, CD_3COCD_3) 47.0. δ_F (376 MHz, CD_3COCD_3) −150.4. ESI-MS (+) m/z: (Lp = $PPyPh_2$, L = chromophore ligand $C_{20}H_{11}$): 1637.146 $[M–BF_4]^+$, 590.014 $[(Lp)AuCu(ACN)(CN)]^+$, 723.141$[(Lp)_2Au]^+$, 1035.044 $[(Lp)_2Au_2Cu(CN)_2]^+$, 1485.211 $[(Lp)_2Au_2(Lc)_2Cu]^+$, 2197.353 $[(Lp)_3Au_3(L)_3Cu]^+$. HR ESI-MS: 1635.1396 $[M–BF_4]^+$, calculated for $C_{74}H_{50}N_2P_2Cu_2Au_2BF_4$: 1635.1408.

Preparation of doped matrixes

The complex-doped film was prepared by drop-casting a mixture of the complex and the corresponding polymer onto a quartz substrate, as detailed here: to prepare the polymer solution, PMMA (MW: 97 000) or PS (MW: 280 000) was dissolved in chloroform at a concentration of 200 mg mL^{-1}. Subsequently, to a 50 μL of polymer solution was added the same volume of a solution of the sample at a concentration of 2 mM. The films were drop cast onto a quartz substrate at room temperature to avoid any thermal annealing.

Conflicts of interest

There are no conflicts to declare.

Data availability

The data supporting the findings of this study, including synthetic procedures, spectroscopic data (NMR, IR, MS), photophysical measurements, and crystallographic information, are available within the article and its supplementary information (SI). Supplementary information: characterization data (NMR, IR, mass spectra); X-ray crystallographic information and packing; photophysical information containing emission quantum yields, lifetimes and absorption and emission complementary figures. See DOI: https://doi.org/10.1039/d6dt00964f.

CCDC 2481587 (**[Au(L)($PPyPh_2$)]**), 2520370 (**Cu1a**) and 2520371 (**Cu1b**) contain the supplementary crystallographic data for this paper.[46a–c]

Acknowledgements

The authors are grateful to projects PID2022-139296NB-I00 funded by the Ministerio de Ciencia, Innovación y Universidades of Spain MCIU/AEI/10.13039/501100011033 and FEDER, UE. This article is based upon work from COST Action CA22131, LUCES Supramolecular LUminescent Chemosensors for Environmental Security, supported by COST (European Cooperation in Science and Technology). The authors also acknowledge the IFARHU-SENACYT program in Panamá for grant no. 270-2022-112 as a Ph.D. Scholarship.

References

1 A. V. Artem'ev, M. P. Davydova, L. S. Klyushova, E. H. Sadykov, M. I. Rakhmanova and T. S. Sukhikh, *Dalton Trans.*, 2024, **53**, 18027.
2 C. Sun, B. K. Teo, C. Deng, J. Lin, G.-G. Luo, C.-H. Tung and D. Sun, *Coord. Chem. Rev.*, 2021, **427**, 213576.
3 C.-H. Huang, M. Yang, X.-L. Chen and C.-Z. Lu, *Dalton Trans.*, 2021, **50**, 5171.
4 J. R. Shakirova, E. V. Grachova, V. V. Gurzhiy, S. Kumar Thangaraj, J. Jãnis, A. S. Melnikov, A. J. Karttunen, S. P. Tunik and I. O. Koshevoy, *Angew. Chem., Int. Ed.*, 2018, **57**, 14154.
5 M. Casciotti, G. Romo-Islas, M. Álvarez, F. Molina, J. M. Muñoz-Molina, T. R. Belderrain and L. Rodríguez, *Dalton Trans.*, 2022, **51**, 17162.
6 A. Pinto, J. S. Ward, K. Rissanen, M. Smith and L. Rodríguez, *Dalton Trans.*, 2022, **51**, 8795.
7 R. K. Gupta, Z. Wang, B. Mohan, C.-H. Tung and D. Sun, *Adv. Funct. Mater.*, 2025, **35**, 2507047.
8 A. de Aquino, N. Santamaria, A. J. Moro, D. Aguilà, A. Prieto, M. C. Nicasio, J. C. Lima and L. Rodriguez, *Inorg. Chem.*, 2025, **64**, 3392.
9 A. Frontera and L. Rodríguez, *Adv. Inorg. Chem.*, 2024, **84**, 55.
10 J. C. Lima and L. Rodríguez, *Adv. Organomet. Chem.*, 2025, **83**, 139.
11 S. Sculfort and P. Braunstein, *Chem. Soc. Rev.*, 2011, **40**, 2741.
12 P. Ai, M. Mauro, L. De Cola, A. A. Danopoulos and P. Braunstein, *Angew. Chem., Int. Ed.*, 2016, **55**, 3338.
13 Q.-C. Peng, Y.-B. Si, Z.-Y. Wang, S.-H. Dai, Q.-S. Chen, K. Li and S.-Q. Zang, *ACS Cent. Sci.*, 2023, **9**, 1419.
14 X. Zhang and H. Xu, *Angew. Chem., Int. Ed.*, 2024, **63**, e202317597.
15 X.-H. Ma, J. Li, P. Luo, J.-H. Hu, Z. Han, X.-Y. Dong, G. Xie and S.-Q. Zang, *Nat. Commun.*, 2023, **14**, 4121.
16 W.-Q. Shi, L. Zeng, R.-L. He, X.-S. Han, Z.-J. Guan, M. Zhou and Q.-M. Wang, *Science*, 2024, **383**, 326.
17 G. Romo-Islas, J. S. Ward, K. Rissanen and L. Rodriguez, *Inorg. Chem.*, 2023, **62**, 8101.
18 I. O. Koshevoy, Y.-C. Chang, A. J. Karttunen, M. Haukka, T. Pakkanen and P.-T. Chou, *J. Am. Chem. Soc.*, 2012, **134**, 6564.
19 A. Yu. Baranov, S. O. Slavova, A. S. Berezin, S. K. Petrovskii, D. G. Samsonenko, I. Yu. Bagryanskaya, V. P. Fedin, E. V. Grachova and A. V. Artem'ev, *Inorg. Chem.*, 2022, **61**, 10925.
20 M. Dahlen, E. H. Hollesen, M. Kehry, M. T. Gamer, S. Lebedkin, D. Schooss, M. M. Kappes, W. Klopper and P. W. Roesky, *Angew. Chem., Int. Ed.*, 2021, **60**, 23365.
21 A. P. Atencio, S. Burguera, G. Zhuchkov, A. de Aquino, J. S. Ward, K. Rissanen, J. C. Lima, I. Angurell, A. Frontera and L. Rodríguez, *Inorg. Chem. Front.*, 2025, **12**, 3041.
22 W.-H. Yu, C. Chen, P. Hu, B.-Q. Wang, C. Redshaw and K.-Q. Zhao, *RSC Adv.*, 2013, **3**, 14099.
23 M. Powers, R. J. Twieg, J. Portman and B. Ellman, *J. Chem. Phys.*, 2022, **157**, 134901.
24 S. Keller, F. Brunner, A. Prescimone, E. C. Constable and C. E. Housecroft, *Inorg. Chem. Commun.*, 2015, **58**, 64.
25 M. Ferrer, A. Gallen, A. Gutiérrez, M. Martínez, E. Ruiz, Y. Lorenz and M. Engeser, *Chem. – Eur. J.*, 2018, **57**, 7346–7354.
26 R. Nandy and S. Sankararaman, *Beilstein J. Org. Chem.*, 2010, **6**, 992.
27 G. F. Manbeck, W. W. Brennessel, R. A. Stockland Jr. and R. Eisenberg, *J. Am. Chem. Soc.*, 2010, **132**, 12307.
28 F. Liu, G. Cao, Z. Feng, Z. Cheng, Y. Yan, Y. Xu, Y. Jiang, Y. Chang, Y. Lv and P. Lu, *ACS Appl. Mater. Interfaces*, 2023, **15**, 47307.
29 M. Ikeda, M. Takeuchi and S. Shinkai, *Chem. Commun.*, 2003, **3**, 1354.
30 R. Nandy and S. Sankararaman, *Org. Biomol. Chem.*, 2010, **8**, 2260.
31 S. K. Petrovskii, A. V. Paderina, A. A. Sizova, A. Y. Baranov, A. A. Artem'ev, V. V. Sizov and E. V. Grachova, *Dalton Trans.*, 2020, **49**, 13430.
32 S. Nayeri, S. Jamali, A. Jamjah and H. Samouei, *Inorg. Chem.*, 2019, **58**, 12122.
33 G. Romo-Islas, S. Burguera, A. Frontera and L. Rodríguez, *Inorg. Chem.*, 2024, **63**, 2821–2832.
34 A. de Aquino, F. J. Caparrós, G. Aullón;, K. N. Truong, K. Rissanen, J. C. Lima and L. Rodríguez, *Dalton Trans.*, 2022, **51**, 16282–16291.
35 A. P. Atencio, A. Sevillano, A. Lázaro, Z. Freixa, D. Aguilà, I. Angurell and L. Rodríguez, *New J. Chem.*, 2025, **49**, 18716.
36 A. de Aquino, F. J. Caparrós, G. Aullón, J. S. Ward, K. Rissanen, Y. Jung, H. Choi, J. C. Lima and L. Rodríguez, *Chem. – Eur. J.*, 2021, **27**, 1810.
37 A. Pinto, A. Llanos, R. M. Gomila, A. Frontera and L. Rodriguez, *Inorg. Chem.*, 2023, **62**, 7131.
38 R. Donamaría, V. Lippolis, J. M. López de Luzuriaga, M. Monge, M. Nieddu and M. E. Olmos, *Inorg. Chem.*, 2018, **57**, 11099.
39 I. S. Krytchankou, D. V. Krupenya, A. J. Karttunen, S. P. Tunik, T. A. Pakkanen, P.-T. Chou and I. O. Koshevoy, *Dalton Trans.*, 2014, **43**, 3383.
40 X.-Y. Chang, G.-T. Xu, B. Cao, J.-Y. Wang, J.-S. Huang and C.-M. Che, *Chem. Sci.*, 2017, **8**, 7815.
41 O. Crespo, M. C. Gimeno, A. Laguna, F. J. Lahoz and C. Larraz, *Inorg. Chem.*, 2011, **50**, 9533.
42 S. Nayeri, S. Jamali, A. Jamjah, J. R. Shakirova, S. P. Tunik, V. Gurzhiy, H. Samouei and H. R. Shahsavari, *Inorg. Chem.*, 2020, **59**, 5702.
43 G. M. Sheldrick, *Acta Crystallogr., Sect. A: Found. Adv.*, 2015, **71**, 3.
44 O. V. Dolomanov, L. J. Bourhis, R. J. Gildea, J. A. K. Howard and H. Puschmann, *J. Appl. Crystallogr.*, 2009, **42**, 339.
45 G. M. Sheldrick, *Acta Crystallogr., Sect. C: Struct. Chem.*, 2015, **71**, 3.
46 (*a*) CCDC 2481587: Experimental Crystal Structure Determination, 2026, DOI: 10.5517/ccdc.csd.cc2p996j; (*b*) CCDC 2520370: Experimental Crystal Structure Determination, 2026, DOI: 10.5517/ccdc.csd.cc2qln88; (*c*) CCDC 2520371: Experimental Crystal Structure Determination, 2026, DOI: 10.5517/ccdc.csd.cc2qln99.